

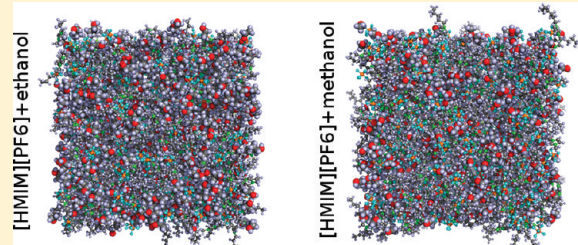
Molecular Dynamics Simulations of the Structural and Thermodynamic Properties of Imidazolium-Based Ionic Liquid Mixtures

T. Méndez-Morales,[†] J. Carrete,[†] O. Cabeza,[‡] L. J. Gallego,[†] and L. M. Varela^{*†}

[†]Grupo de Nanomateriales y Materia Blanda, Departamento de Física de la Materia Condensada, Universidad de Santiago de Compostela, Campus Vida, s/n, E-15782 Santiago de Compostela, Spain

[‡]Facultad de Ciencias, Universidade de A Coruña, Campus A Zapateira s/n, E-15008, A Coruña, Spain

ABSTRACT: In this work, extensive molecular dynamics simulations of mixtures of alcohols of several chain lengths (methanol and ethanol) with the ionic liquids (ILs) composed of the cation 1-hexyl-3-methylimidazolium and several anions of different hydrophobicity degrees (Cl^- , BF_4^- , PF_6^-) are reported. We analyze the influence of the nature of the anion, the length of the molecular chain of the alcohol, and the alcohol concentration on the thermodynamic and structural properties of the mixtures. Densities, excess molar volumes, total and partial radial distribution functions, coordination numbers, and hydrogen bond degrees are reported and analyzed for mixtures of the ILs with methanol and ethanol. The aggregation process is shown to be highly dependent on the nature of the anion and the size of the alcohol, since alcohol molecules tend to interact predominantly with the anionic part of the IL, especially in mixtures of the halogenated IL with methanol. Particularly, our results suggest that the formation of an apolar network similar to that previously reported in mixtures of ILs with water does not take place in mixtures with alcohol when the chloride anion is present, the alcohol molecules being instead homogeneously distributed in the polar network of IL. Moreover, the alcohol clusters formed in mixtures of [HMIM][PF₆] with alcohol were found to have a smaller size than in mixtures with water. Additionally, we provide a semiquantitative analysis of the dependence of the hydrogen bonding degree of the mixtures on the alcohol concentration.



1. INTRODUCTION

Room temperature ionic liquids (ILs) are novel compounds that have been widely analyzed in the last two decades. Because of some unique properties, such as low vapor pressure, stability of their liquid state over a large temperature interval (around 300 °C), nonflammability, nonvolatility, or solubility in a wide range of organic solvents,^{1–5} they have many applications as “green solvents” and have been considered as an alternative to common organic solvents.^{6–8} These systems are, in general, composed of an organic cation and a monatomic or polyatomic inorganic or organic anion such as PF_6^- , BF_4^- , Cl^- , Br^- , NTf_2^- , and so forth. Physicochemical properties (viscosity, hydrophobicity, toxicity, catalytic activity, etc.) of ILs can be made to vary broadly by an appropriate selection of cations and anions; for this reason, and taking into account their huge estimated⁹ number (10^{18}), they are considered “designer” solvents.¹⁰

For the further development of applications of ILs as solvents, knowledge of their physicochemical properties, and those of their mixtures with both inorganic and organic compounds (mainly water and alcohols) is of crucial importance. For this purpose, it is particularly relevant to understand how the structure and properties of IL mixtures change upon mixing, as well as the dependence of the properties of the resulting mixtures on their composition.

The interaction between ILs and polar or apolar solvents has been investigated by means of molecular simulation and

experimental studies before. However, contrarily to the case of IL/water mixtures, for which the number of reported contributions has greatly increased over the last years (see, for example, refs 11 and 12 and references therein), studies of mixtures with alcohol are still scarce. In this latter case, some experimental results^{13–23} have been reported during the past decade. Particularly, several works have been done studying the factors that govern the phase behavior of imidazolium based ILs in different systems.^{13–15} For instance, Crosthwaite et al.¹⁵ carried out a systematic study of the effect of different characteristics of the components on the liquid equilibrium of IL/alcohol mixtures. They reported results similar to those of Pereiro and Rodríguez,¹⁶ whose solubility studies show that the immiscibility range of IL/alcohol binary systems decreases with an increase in the IL alkyl chain length. These results are compatible with those of Domanska et al.,¹⁷ who determined that the solubility of ILs in alcohols decreases with an increase in the length of the molecular chain of the alcohol. Moreover, Pereiro and Rodríguez’s results suggest that a replacement of the hydrogen at the C2 position of the imidazolium ring with a methyl group causes an increase in the upper critical solution temperature, whereas the choice of the

Received: July 5, 2011

Revised: August 20, 2011

Published: September 07, 2011

anion has a great impact on this property, and its effect is related to the ability of the anion to form a hydrogen bond. Several experimental studies have also been performed with the aim of studying thermodynamic properties of mixtures of imidazolium-based ILs with alcohols, such as densities and excess molar volumes, refractive indices, speed of sound, or surface tension.^{18–23} As an example, Cabeza and co-workers²³ studied the influence on surface tension and density of the alkyl chain length of the IL family 1-alkyl-3-methylimidazolium tetrafluoroborate ($[AMIM][BF_4]$) with water and ethanol. The results obtained show a monotonic decrease of the density of the mixtures with increasing ethanol (or water) molar fraction, and a decrease of the surface tension with the increase of the alkyl chain length of the IL cation.

As it is usually very complicated to experimentally investigate the behavior of ILs at the atomic level, molecular dynamics (MD) simulations are usually the best way to probe the properties of the mixtures. In fact, a great number of simulation studies have been dedicated over the past years to investigate the thermodynamic and structural properties of both pure ILs and of IL/solvent mixtures. However, the truth is that mixtures have received much less attention. Up to now, the most studied among IL mixtures have been those with water. In 2003, Hanke and Lynden-Bell²⁴ reported the first, as far as we know, MD study of both the local structure and dynamics of mixtures of water with two ILs, 1,3-dimethyl imidazolium chloride ($[DMIM][Cl]$) and 1,3-dimethyl imidazolium hexafluorophosphate ($[DMIM][PF_6]$). Jiang et al.²⁵ investigated the influence of water concentration on the nanostructural organization in mixtures of 1-octyl-3-methylimidazolium nitrate ($[OMIM][NO_3]$) with water. Feng and Voth²⁶ reported very recently the first (to our knowledge) MD study of the effect of both alkyl chain length and anion on the structure and dynamics of IL/water mixtures. They analyzed three IL/water mixtures at several water mole fractions: 1-butyl-3-methylimidazolium tetrafluoroborate ($[BMIM][BF_4]$), 1-octyl-3-methylimidazolium tetrafluoroborate ($[OMIM][BF_4]$) and 1-octyl-3-methylimidazolium chloride ($[OMIM][Cl]$). We have also recently reported systematic MD simulations of the structure and dynamics of mixtures of water with several imidazolium-based ILs.¹¹ In particular, we analyzed radial distribution functions, coordination numbers, hydrogen bonding degrees, mean squared displacements, self-diffusion coefficients, and, for the first time, the velocity autocorrelation function of water molecules in the mixture.

In what IL/alcohol mixtures are concerned, the reported results are much scarcer. Hanke et al.²⁷ reported a computational study of mixtures of $[DMIM][Cl]$ with water, methanol, dimethyl ether, and propane. They found that the strongest solute–solvent interactions in water and methanol mixtures are hydrogen bonding of water and methanol with the IL anion, whereas for dimethyl ether and propane, interactions with the imidazolium cations are more important. In 2006, Canongia-Lopes et al.²⁸ analyzed the solvation of nonpolar, polar and associating solutes in 1-butyl-3-methylimidazolium hexafluorophosphate ($[BMIM][PF_6]$) in mixtures with *n*-hexane, acetonitrile, methanol, and water. These authors confirmed the presence of segregated polar and nonpolar domains in the bulk mixtures. Additionally, Raabe and Köhler²⁹ reported a computational study of binary mixtures of ILs of the 1-alkyl-3-methylimidazolium chloride ($[AMIM][Cl]$) IL family with ethanol and 1-propanol to calculate their densities, excess energies of mixing, and structural properties such as radial and spatial distribution functions. On the other hand, Jahangiri et al.³⁰ performed MD simulations of the mixture of 1-ethyl-3-methylimidazolium chloride ($[EMIM][Cl]$) and 1-ethyl-3-methylimidazolium hexafluorophosphate

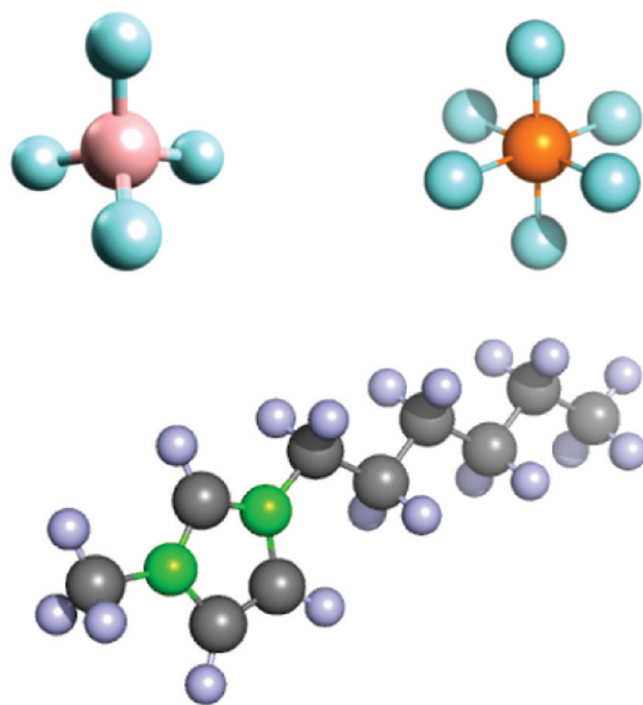


Figure 1. Molecular structures of $HMIM^+$, PF_6^- , and BF_4^- ions.

($[EMIM][PF_6]$) with both methanol and ethanol in order to investigate excess properties and some physical and structural properties of the mixture, such as excess enthalpies, excess volumes, radial distribution functions, cohesive energy density, and diffusion coefficients. More recently, Heintz et al.³¹ reported MD simulations to calculate tracer diffusion coefficients of the IL ions in mixtures of 1-ethyl-3-methylimidazolium bis(trifluoromethanesulfonyl)imide ($[EMIM][NTf_2]$) and 1-butyl-3-methylimidazolium bis(trifluoromethanesulfonyl)imide ($[BMIM][NTf_2]$), both with water and methanol.

A detailed knowledge and understanding of the physicochemical properties of alcohol/IL mixtures is of fundamental importance to further explore the great number of potential academic, industrial, and biomedical applications of ILs. However, a systematic study of the relation between the structure and the properties of the mixture, including the role of different parameters such as cation length, anion, composition and alcohol chain size, is not available at this point. As it is well-known,^{32,33} the length of the imidazolium cation chain is directly related to the hydrophobicity of ILs, (the longer the chain, the more hydrophobic the IL), and consequently it is expected to have a deep impact on the properties of their mixtures. However, the role of the anion is not completely understood, although the expected tendency is an increase of the solvophobicity with the presence of larger anions (such as PF_6^-) instead of monatomic anions (such as Cl^-). In IL–water mixtures, the anion is known to be the most influential entity on the properties of the polar network in the bulk mixture, and it is also known to be an important factor in determining ILs solubility in water and alcohols. Moreover, in order to rationalize the behavior of IL–alcohol mixtures it is of fundamental importance to know how the latter compound takes part in the solvation process of ILs. In this work we performed extensive MD simulations to investigate several thermodynamic and structural properties of mixtures of alcohols and 1-hexyl-3-methylimidazolium ($HMIM^+$) with three different anions of

various solvophilic degrees: Cl^- , the one with the larger effect on water structure according to the Hoffmeister series; the highly hydrophobic PF_6^- , with low miscibility with water; and BF_4^- , with intermediate characteristics (see Figure 1). The chosen alcohols were methanol and ethanol, in order to investigate and compare the influence of the length of the molecular chain of the alcohol in the properties of the mixtures. Moreover, we analyzed the impact of the anion nature and alcohol concentration on the microstructure of the mixtures by analyzing their densities, excess molar volumes, radial distribution functions, coordination numbers, and degrees of hydrogen bonding.

The remainder of this paper is organized as follows. In section 2 we give details of the computational procedure used in our study; in section 3 we present and discuss the obtained results, and, in section 4 we summarize our main conclusions.

2. SIMULATION DETAILS

The MD simulations for pure ILs and their mixtures with alcohols were performed using the Gromacs package.³⁴ All the simulations were run at 298.15 K, and the analyzed mole fractions of alcohol in the IL/alcohol mixtures were $x_{\text{alcohol}} = \{0.00, 0.10, 0.20, 0.30, 0.40, 0.50, 0.60, 0.70, 0.80, 0.90, 0.95, 0.98, \text{ and } 1.00\}$, as both ethanol and methanol are miscible with all the selected ILs ([HMIM][PF₆], [HMIM][BF₄] and [HMIM][Cl]) throughout the whole concentration range.^{16,22,23} The number of IL molecules in the cubic box was set to 300, except for $x_{\text{alcohol}} = 0.10$, where we considered 450 IL molecules in order to have enough alcohol to yield statistically significant trajectories, $x_{\text{alcohol}} = 0.95 - 0.98$, where just 50 ionic pairs were introduced so as to keep the system size small enough, and $x_{\text{alcohol}} = 1.00$, a case in which only alcohol molecules are present. The number of alcohol molecules was adjusted in each situation counting each ionic pair as a single molecule in the calculation of mole fractions.

The parametrization of the ions was carried out in the framework of the OPLS force field developed by Jorgensen and co-workers³⁵ for different organic fluids. In the functional form of the OPLS force field in eq 1, the first three terms represent the bonded interactions, i.e., bonds, angles, and torsions, while the nonbonded interactions are described by the last two terms, and include van der Waals and Coulombic interactions:

$$\begin{aligned} E = & \sum_i K_{b,i} [r_i - r_{0,i}]^2 + \sum_i K_{b,i} [\theta_i - \theta_{0,i}]^2 \\ & + \sum_i \left[\frac{1}{2} V_{1,i} (1 + \cos \varphi_i) + \frac{1}{2} V_{2,i} (1 + \cos 2\varphi_i) \right. \\ & \left. + \frac{1}{2} V_{3,i} (1 + \cos 3\varphi_i) + \frac{1}{2} V_{4,i} (1 + \cos 4\varphi_i) \right] \\ & + \sum_i \sum_{j < i} \left\{ \frac{1}{4\pi\epsilon_0} \frac{q_i q_j e^2}{r_{ij}} + 4\epsilon_{ij} \left[\left(\frac{\sigma_{ij}}{r_{ij}} \right)^{12} - \left(\frac{\sigma_{ij}}{r_{ij}} \right)^6 \right] \right\} \end{aligned} \quad (1)$$

The parameters used in the above equation are the force constants K , the reference values r_0 and θ_0 , the Fourier coefficients V , and the partial atomic charges q . σ_{ij} and ϵ_{ij} represent the Lennard-Jones radii and potential well depths, respectively, which are obtained from parameters for each type of atom using geometric combination rules $\sigma_{ij} = (\sigma_{ii}\sigma_{jj})^{1/2}$ and $\epsilon_{ij} = (\epsilon_{ii}\epsilon_{jj})^{1/2}$. As it is known, there are both united atom (OPLS-UA) and all-atom (OPLS-AA) versions of the OPLS force field. The former

includes hydrogen atoms bonded to carbon implicitly in the carbon parameters, and in the latter every hydrogen atom is modeled explicitly. The cations were modeled using the all-atom representation of the CH₂ and CH₃ groups in the alkyl chain, as well as that of the methyl group attached to the imidazolium ring. As for the anions, PF₆⁻ was modeled as a set of seven sites with partial charges of 1.34 for the phosphorus atom and -0.39 for the fluorine atoms.³⁶ BF₄⁻ was modeled as a set of five sites with partial charges of 1.176 for the boron atom and -0.544 for the fluorine atoms,³⁷ while Cl⁻ was modeled by a single site of charge -1.³⁸ Among the partial charges used, those taken from the work by Acevedo and Canongia-Lopes et al. (refs 36 and 38, respectively) come from application of the restrained electrostatic potential (RESP) fitting method,³⁹ while the ones reported by Prado and Freitas in ref 37 were computed by MP2/6-31 g(d) using the ChelpG methodology⁴⁰ implemented in the GAUSSIAN 94 package.⁴¹ The force field parameters of HMIM⁺, including partial charges, were taken from the development of OPLS-AA parameters for 68 combinations of ILs reported in ref 36. On the other hand, ethanol and methanol molecules were represented by the molecular model proposed by Jorgensen.⁴² Long-range electrostatic interactions were processed using the particle-mesh Ewald (PME)⁴³ method with a grid spacing of 0.12 nm and cubic interpolation. The cutoff distance for Lennard-Jones interactions was set to 1.1 nm, and a search of neighbors was made up to this same distance from the central ion and was updated every five simulation steps. The Linear Constraint Solver (LINCS) algorithm^{44,45} with a fourth-order expansion of the constraint coupling matrix was used to constrain the bonds, and long-range dispersion corrections were used for energy and pressure.

Initial configurations were energy-minimized for 10⁶ steps using a conjugated gradients algorithm in order to remove bad contacts resulting from the initial random configuration of ions. The maximum step size and the tolerance were set to 0.01 nm and 0.1 kJ·nm⁻¹·mol⁻¹, respectively. The equilibration phase was performed in the isothermal-isobaric (N, p, T) ensemble during 100 ps to ensure the full equilibration of all the properties of the system. For any given system, an appropriate choice of equilibration time depends on the complexity of the simulated molecules, their relative masses and the parameters of the thermostat and barostat, as well as on the temperature and density at equilibrium. In particular, our experience shows that, in contrast with other cases where several more conformationally complex molecules (such as proteins) are involved, for imidazolium-based ILs, 100 ps is usually considered to be enough.⁴⁶ In our simulations, as a criterion for equilibration we checked that all thermodynamic properties (except for pressure, which shows the expected very large short-term fluctuations usually present in this kind of simulations) were stable. The results of an additional 2000-ps simulation in the isothermal-isobaric ensemble were used for analysis. The temperature control was implemented using the V-rescale thermostat.⁴⁷ Cations and anions (and alcohols in those cases where we include a solvent) were separated into two (three) baths with temperature coupling constants of 0.1 ps. The pressure control was set using a Parrinello-Rahman barostat⁴⁸ with a reference pressure of 1 atm, an isothermal compressibility of 4.5×10^{-5} bar⁻¹, and a relaxation time of 1.0 ps.

Each of these simulations provided us with a sequence of configurations, i.e., positions and instantaneous velocities of all atoms of the system, which was analyzed to obtain structural and thermodynamic information about the aforementioned mixtures.

Table 1. Simulated and Experimental Densities and Experimental Molar Volumes for Pure ILs and Alcohols at 298.15 K, and Deviations from Experimental Data

compound	ρ_{sim} (kg/m ³)	ρ_{exp} (kg/m ³)	$\Delta\rho$ (%)	V_m (cm ³ /mol)
[HMIM][PF ₆]	1270.5 ± 4.9	1293.7	1.79	241.32
[HMIM][BF ₄]	1128.6 ± 4.6	1145.4	1.47	221.83
[HMIM][Cl]	1034.4 ± 3.9	1040.4	0.57	194.86
Methanol	776.7 ± 5.9	786.0	1.19	40.76
Ethanol	796.6 ± 9.5	785.4	1.42	58.66

3. RESULTS AND DISCUSSION

Density of ILs is one of the most reliable sources of experimental data, therefore comparisons between experimental and computational results for liquid densities are usually used to estimate the accuracy of the force field employed in MD simulations.^{26,29} Densities of pure ILs and alcohols obtained from MD simulations, as well as their comparison with experimental data and the respective deviations, are shown in Table 1. The reported MD simulations of pure ILs at 298.15 K show underestimations of experimental densities^{16,22,23} ranging from 0.6% to 1.8%. Moreover, the comparison of our simulated densities of pure alcohols with the experimental data^{22,42} exhibits an underestimation of 1.2% for methanol and an overestimation of 1.4% for ethanol, both at 298.15 K. Thus, we could say that our presently reported MD density results for pure ILs and pure alcohols are in good agreement with the experimental ones. These results allow us to be reasonably confident in our simulation model and, consequently, in the calculated densities of the IL/alcohol mixtures, for which (to our knowledge) no MD results have been reported so far.

Our computational results for the density over the whole composition range of the binary mixture [HMIM][PF₆]/ethanol at 298.15 K are shown in Figure 2a together with the experimental results reported by Pereiro and Rodríguez.¹⁶ As can be seen there, the predictions for the density of [HMIM][PF₆]/ethanol mixtures are in excellent agreement with the experimental values. All the other mixtures showed the same tendency as this one, a monotonic decrease from the density of pure IL to that of pure alcohol with an increase of alcohol concentration, and their predicted densities were also in excellent agreement with the experimental values. It is noteworthy that this behavior is in marked contrast to that previously reported on mixtures of our halogenated IL with water, for which Gómez et al.^{22,49} reported that its binary mixtures with water present a maximum value of the density at $x_{\text{water}} \approx 0.5$. In this sense, one must recall that water is known to be the only molecular compound in which the existence of thermodynamic anomalies such as density maxima and a liquid–liquid phase transition is firmly established.⁵⁰ Thus, the density maximum in [HMIM][Cl]/water mixtures can be due to some structural transition in the associated to the formation of continuous networks of water during the transition from the ionic to the polar network, which does not take place in the case of mixtures with alcohol.

Additionally, the excess molar volumes of the mixtures were calculated from their density values through the well-known eq 2:

$$V_m^E = \sum_{i=1}^2 x_i M_i (\rho^{-1} - \rho_i^{-1}) \quad (2)$$

where ρ and ρ_i stand for the density of the mixture and the density of the pure components, respectively, x_i represents the

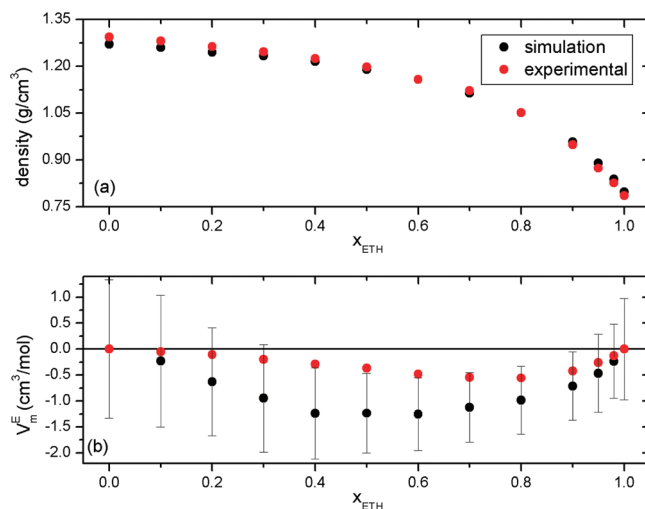


Figure 2. (a) Comparison between simulated (black dots) and experimental (red dots) densities of a [HMIM][PF₆]/ethanol mixture at 298.15 K, and (b) comparison between simulated (black dots) and experimental (red dots) excess molar volumes calculated from densities data of a [HMIM][PF₆]/ethanol mixture at 298.15 K; both as a function of the ethanol mole fraction. Experimental results were reported by Pereiro and Rodríguez.¹⁶

mole fraction of the i th component of the mixture, and M_i is its molar mass. Figure 2b shows a comparison between the calculated excess molar volumes and the experimental ones reported by Pereiro and Rodríguez in ref 16 for the binary mixture of [HMIM][PF₆] with ethanol at 298.15 K as a function of ethanol mole fraction. It is noteworthy that the relative reported experimental excess molar volumes for IL/alcohol mixtures are less than 0.5% of the molar volumes of the pure components (see Table 1), indicating the quasi ideal behavior of these systems.²³ It can be seen there that our simulations overestimate the excess molar volume by $\sim 1 \text{ cm}^3/\text{mol}$, but the experimental values lie within the uncertainty intervals as represented by the error bars calculated by propagating the uncertainties of the stochastic series of simulated densities, whose uncertainties are given by Gromacs by calculating the dispersion of the density around its average value. As a matter of fact, it is extremely difficult to obtain V_m^E with accuracy from a simulation, given that very small differences in density can induce large differences in excess molar volume. Indeed, the same behavior was reported by Kelkar et al.,⁵¹ who concluded that the simple point charge (SPC) model of water overestimates excess molar volumes by $\sim 1 \text{ cm}^3/\text{mol}$ in mixtures of 1-ethyl-3-methylimidazolium ethylsulfate ([EMIM][EtSO₄]) with water. Moreover, it can be seen in Figure 3 that the excess molar volumes are negative over the entire composition range for the binary mixtures, both in mixtures with ethanol and in those with methanol, in good agreement with experimental and computational results previously reported in the literature for IL/alcohol mixtures.^{16,18,19,22} Hence, all the studied compounds show a contractive tendency upon mixing, and all of them reach a minimum at x_{alcohol} between 0.4 and 0.7. As it is well-known, the association trend on mixtures depends on the intermolecular forces between the components of the mixture, and the packing effect due to the different shapes and sizes of the molecules. In this case, the ion-dipole interactions between alcohol molecules and the IL ions are stronger than the interactions between the molecules in the pure components, so the

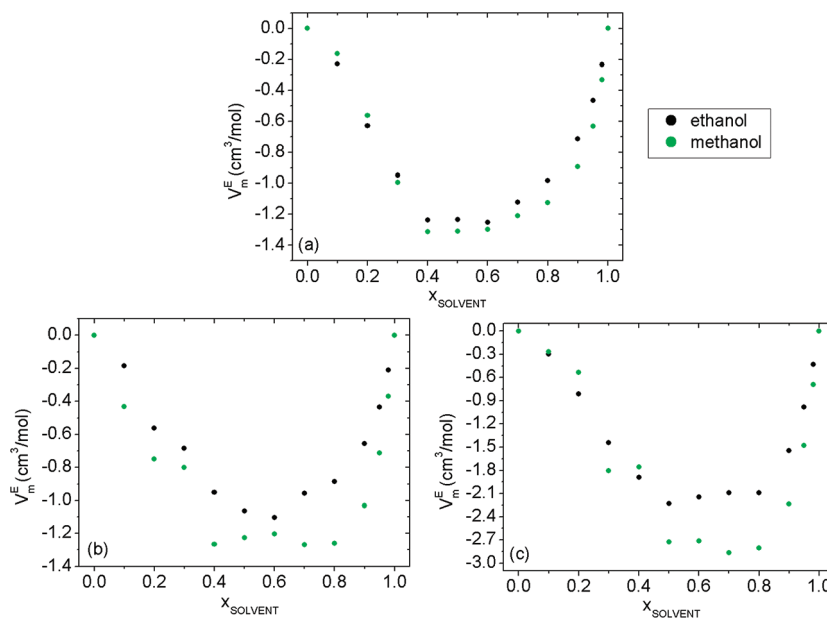


Figure 3. Excess molar volumes calculated from our computational results for the densities of (a) $[\text{HMIM}][\text{PF}_6]$ /alcohol, (b) $[\text{HMIM}][\text{BF}_4]$ /alcohol, and (c) $[\text{HMIM}][\text{Cl}]$ /alcohol (green dots correspond to methanol, and black dots correspond to ethanol) mixtures at 298.15 K as a function of the alcohol mole fraction.

excess molar volumes become slightly negative. Our calculated absolute values of V^E are larger in the case of mixtures of $[\text{HMIM}][\text{Cl}]$ with both alcohols (Figure 3c), reaching values twice as large as those obtained for PF_6^- and BF_4^- (Figure 3a,b, respectively), which were similar to each other. This indicates that more alcohol molecules fit into the free volume between the ions of ILs in the case of mixtures with chloride than in the mixtures with the biggest anions. Thus, anions exert a deep impact on mixing, and hydrophilic ILs seem to have greater miscibility with methanol and ethanol than the hydrophobic ones. Moreover, the minimum of our calculated excess molar volume is more negative in mixtures with methanol than in mixtures with ethanol, showing a better packing for smaller molecular chain of the alcohol. Considering the predictions for the densities and excess molar volumes of the studied mixtures, we can conclude that the simulation model predicts reasonably well the thermodynamic properties of the system. In the following, we will apply it to the study of the microscopic structure of these mixtures.

The structure of dense fluids is usually characterized by means of the radial distribution function (RDF) defined as

$$g(r) = \frac{1}{\rho N} \left\langle \sum_{ij} \delta(r - r_{ij}) \right\rangle \quad (3)$$

where N is the number of particles in the system, ρ stands for its number density, i and j run over all system particles, and brackets indicate ensemble average. All RDFs presented in this paper (unless otherwise noted) were calculated using the center of mass of the anions and the center of mass of the imidazolium ring of the cation. Our computational ion–ion RDFs for pure ILs are shown in Figure 4, where the influence of the anion on the structure of the system is analyzed. Most remarkably, the first peak of the cation–anion RDF for the halogen anion is notably higher than those obtained for the PF_6^- and BF_4^- anions (Figure 4a), and it is placed at smaller distances (0.45 nm)

with respect to the polyatomic anions (0.53 nm for PF_6^- and 0.50 nm for BF_4^-), probably due to the bigger size of the fluorinated anions. For the same reason, the maximum of the first peak of the cation–anion BF_4^- RDF is registered at a slightly lower distance than that for the PF_6^- anion. Moreover, all cation–anion RDFs show a shoulder at the end of their first peaks of the cation–anion RDF, which is more prominent in the presence of the chloride ion (at 0.57 nm), and much more imperceptible for the more hydrophobic anions. These features have also been observed in some liquids such as Ga, Si, Sn, or Bi (see ref 52 and references therein), where it has been interpreted as a signature of a short-lived diatomic molecular unit, and also in IL/water mixtures.¹¹ Contrary to what happens with this first peak, the impact of the variation of the anion in the distribution of higher order neighbors seems to be relatively limited. On the other hand, the cation–cation RDF (Figure 4b) for the halogen anion shows a first peak around 0.40 nm, but similar features are almost invisible in $[\text{HMIM}][\text{PF}_6]$ and $[\text{HMIM}][\text{BF}_4]$. Regarding the anion network structure, we see that a double first peak is obtained for PF_6^- and BF_4^- anions, centered at 0.80 and 0.75 nm, respectively; while the anion–anion RDF of $[\text{HMIM}][\text{Cl}]$ exhibits a single peak around 0.70 nm. These results are in agreement with the features reported in our previous work about IL/water mixtures,¹¹ in which the GROMOS96 43A1 force field was used.

In order to analyze the alcohol distribution in bulk mixtures, we calculated alcohol–alcohol, cation–alcohol, and anion–alcohol RDFs in IL/alcohol mixtures, and they are shown in Figures 5, 6, and 7, respectively. In the first one, ethanol–ethanol RDFs (Figure 5a,c,e) exhibit a first peak at approximately 0.47 nm, with a maximum height of approximately 2.3 in the $[\text{HMIM}][\text{PF}_6]$ and $[\text{HMIM}][\text{Cl}]$ mixtures (Figure 5a,e), at the lowest concentration of ethanol. However, the smallest quantity of ethanol in mixtures with $[\text{HMIM}][\text{BF}_4]$ (Figure 5c) shows the lowest peak of the whole concentration range of that mixture, its value being less than 1.4. In general, the first peak of ethanol–ethanol RDFs decreases with increasing ethanol mole fraction, indicating that

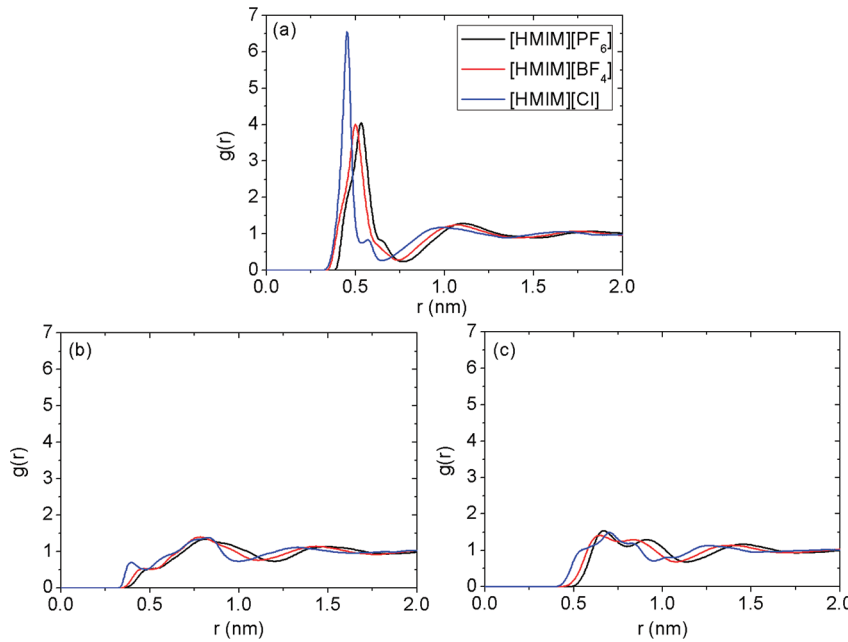


Figure 4. RDFs for cation–anion (a), cation–cation (b), and anion–anion (c) of HMIM^+ with three different counterions (PF_6^- , BF_4^- , and Cl^-) at 298.15 K and 1 atm.

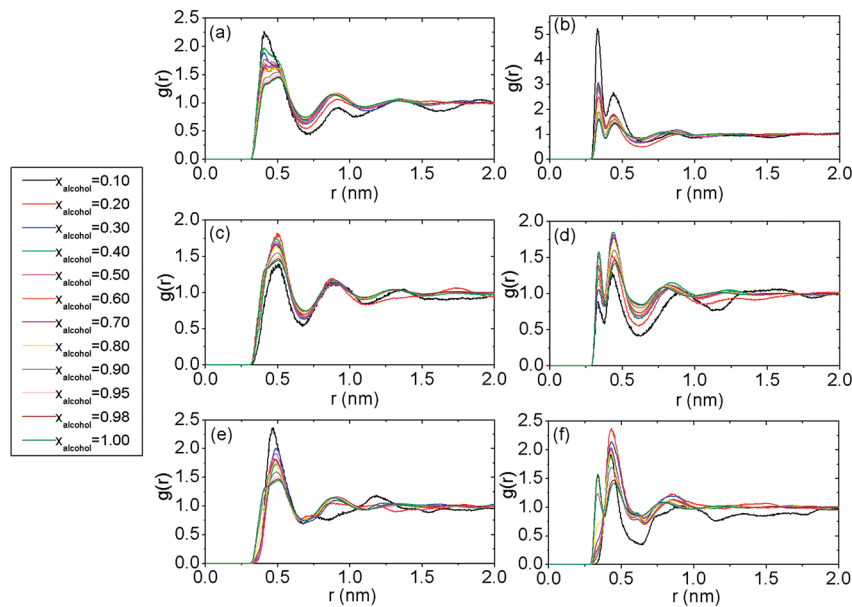


Figure 5. Alcohol mole fraction dependence of ethanol–ethanol (a,c,e) and methanol–methanol (b,d,f) RDFs for $[\text{HMIM}]^+ \text{[PF}_6^-]$ (a,b), $[\text{HMIM}]^+ \text{[BF}_4^-]$ (c,d), and $[\text{HMIM}]^+ \text{[Cl}^-]$ (e,f) at 298.15 K and 1 atm.

spatial correlation between ethanol molecules decreases when ethanol concentration increases, but there are some exceptions that show an inversion, such as $x_{\text{ethanol}} = 0.2$ in the $[\text{HMIM}]^+ \text{[PF}_6^-]$ /ethanol mixture, $x_{\text{ethanol}} = 0.3$ in the $[\text{HMIM}]^+ \text{[BF}_4^-]$ /ethanol one, or $x_{\text{ethanol}} = 0.2$ and $x_{\text{ethanol}} = 0.4$ in the $[\text{HMIM}]^+ \text{[Cl}^-]$ /ethanol mixture. On the other hand, methanol–methanol RDFs (Figure 5b,d,f) show a double first peak, the first one (sharper in the case of $[\text{HMIM}]^+ \text{[PF}_6^-]$ in Figure 5b) at 0.33 nm, and the second one (sharper in the cases of $[\text{HMIM}]^+ \text{[BF}_4^-]$ and $[\text{HMIM}]^+ \text{[Cl}^-]$ in Figure 5d,f, respectively) at 0.44 nm in all cases. It can be deduced that methanol molecules are distributed in two nearby shells

around other methanol molecules, whereas ethanol molecules are distributed in two further shells (the center of the second shell is placed at 0.88 nm in mixtures with ethanol) and the peaks corresponding to third neighbors can be neglected. Moreover, it can be seen that RDFs of the methanol/ $[\text{HMIM}]^+ \text{[Cl}^-]$ mixture only show the first peak when $x_{\text{methanol}} = 0.9$ is reached, showing that the halogen anion prevents the formation of the first methanol layer. Furthermore, the second peak decreases with increasing methanol mole fraction, showing exceptions at $x_{\text{methanol}} = 0.1$ and $x_{\text{methanol}} = 0.4$. For methanol/ $[\text{HMIM}]^+ \text{[BF}_4^-]$ mixtures, the spatial correlation of methanol molecules increases with an increase of the

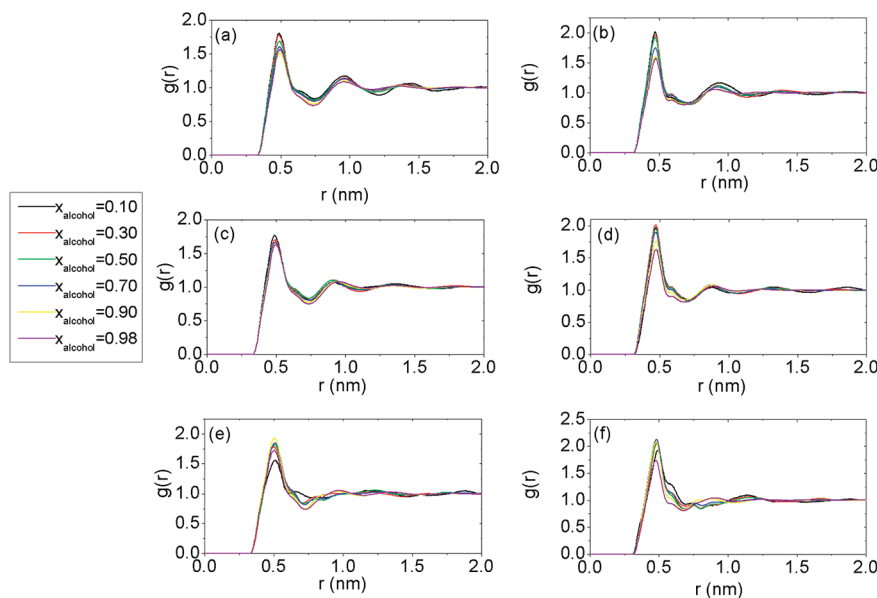


Figure 6. Alcohol mole fraction dependence of cation–ethanol (a,c,e) and cation–methanol (b,d,f) RDFs for [HMIM][PF₆] (a,b), [HMIM][BF₄] (c,d), and [HMIM][Cl] (e,f) at 298.15 K and 1 atm.

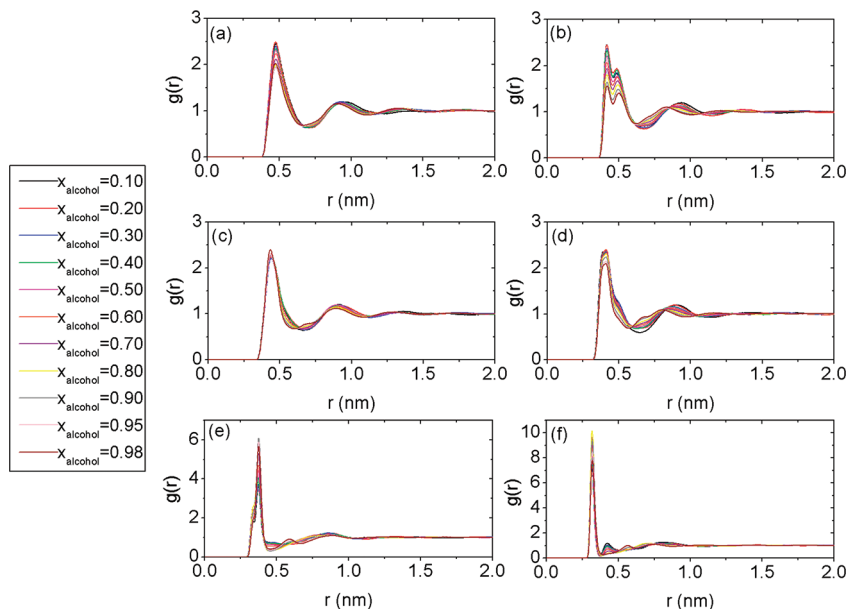


Figure 7. Alcohol mole fraction dependence of anion–ethanol (a,c,e) and anion–methanol (b,d,f) RDFs for [HMIM][PF₆] (a,b), [HMIM][BF₄] (c,d), and [HMIM][Cl] (e,f) at 298.15 K and 1 atm.

mole fraction of alcohol, with an inversion at $x_{\text{methanol}} = 0.3$. The RDFs in Figure 5b reach the highest maximum for the lower concentration of methanol in [HMIM][PF₆], with a value of approximately 5. From this representation we can infer that methanol molecules are more clusterized than ethanol ones when the hydrophobic anion is present, and that the height of this first peak decreases with increasing methanol mole fraction. However, the fact that highest peaks reach much lower values than those reported in our previous work for mixtures of [HMIM][PF₆] with water¹¹ allows us to deduce that the clusterization degree of methanol in mixtures with [HMIM][PF₆] is much lower than the clusterization degree of water in mixtures with the same IL.

However, it is still higher than in mixtures of methanol with [HMIM][BF₄] or [HMIM][Cl]. In this same way, Raabe and Köhler²⁹ concluded that in binary mixtures of [AMIM][Cl] with ethanol and propanol, a continuous solvent network similar to that found in water/IL mixtures (see refs 11 and 24–26) is not present, and that the alcohol seems to be homogeneously distributed in the cation–anion network of the IL.

Figure 6 illustrates the cation–alcohol RDFs in the studied mixtures. For clarity, only a few of all the analyzed mole fractions are shown. In all the cases shown in Figure 6, one can observe a first peak around 0.48 nm, which slightly decreases with an increase of the mole fraction of alcohol (except in [HMIM][Cl]/ethanol

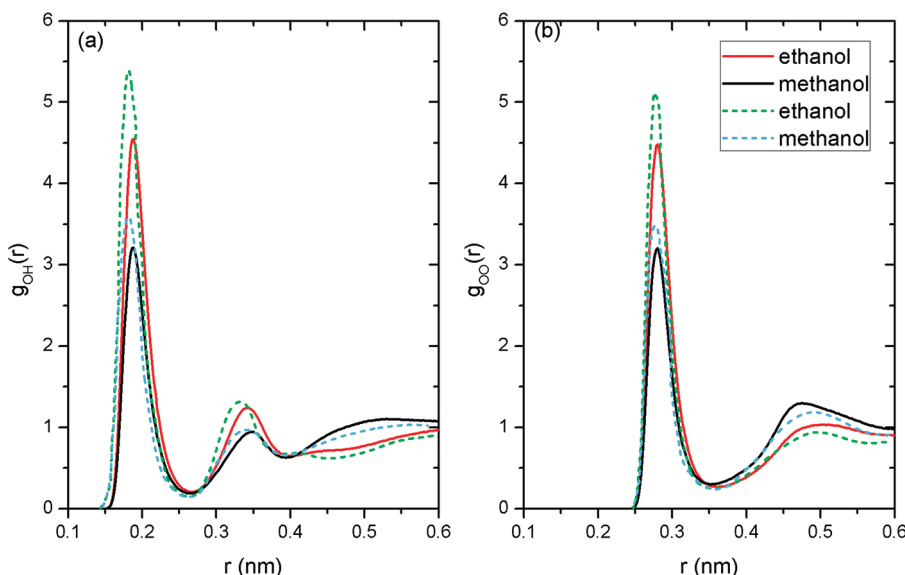


Figure 8. RDFs for ethanol (red lines) and methanol (black lines) at 298.15 K, and comparison with the curves reported by Saiz et al. (dashes).⁵²

mixtures, where it shows the opposite tendency). In mixtures with both polyatomic anions (Figure 6a–d), a second peak can be identified around 0.90 nm, whereas when chloride is present, cation–alcohol RDFs quickly converge to the ideal value for both alcohols. The fact that the first peak height is lower than 2 and that the RDFs are quickly smoothed out implies that there is no aggregation of alcohol molecules around the cations of ILs. This behavior was also reported by Jahangiri et al.³⁰ in mixtures of methanol with [EMIM][PF₆] and [EMIM][Cl].

The situation is completely different for the anion–alcohol RDFs shown in Figure 7. For the ethanol molecules around PF₆⁻ (Figure 7a) there is a peak at 0.47 nm, whereas, in the case of methanol (Figure 7b) there are two peaks, the first one at 0.42 nm being sharper and the second one around 0.50 nm broader. In both mixtures with [HMIM][BF₄] (Figure 7c,d) the first peak of anion–alcohol RDFs is placed at shorter distances than in the case with PF₆⁻, at 0.43 nm for the mixture with ethanol and at 0.40 nm for the system with methanol. In the case of methanol/[HMIM][BF₄] mixtures, the second peak found in the presence of the PF₆⁻ anion is absent. Regarding mixtures of alcohols with [HMIM][Cl] (Figure 7e,f), both RDFs show a high and sharp first peak, around 0.37 nm in mixtures with ethanol and at 0.33 nm in those with methanol. The height of these two peaks is higher in the case of the shorter alcohol, which implies that there is a stronger interaction of Cl⁻ with methanol than with ethanol. Moreover, it can be seen from Figure 7e,f that this first peak of the anion–alcohol RDFs remains at the same position, but the height of the peaks increases with the increase of the mole fraction of alcohol, as was also reported in refs 29 and 30. However, this behavior is in contrast to our previous results for [HMIM][Cl]/water mixtures,¹¹ in which we reported that the structuring was weakened as water concentration increased. Moreover, the height of the highest peak in methanol/[HMIM][Cl] mixtures (corresponding to $x_{\text{methanol}} = 0.8$) is lower than the highest peak in water/[HMIM][Cl] mixtures (corresponding to $x_{\text{water}} = 0.1$), their values being around 10 and 15, respectively. In [HMIM][Cl]/methanol mixtures (Figure 7f), a melt second peak appears around 0.43 nm illustrating the establishment of a second solvation shell of methanol molecules placed around the

halogen anion. This peak of second neighbors around the anion was also observed by Raabe and Köhler.²⁹ The maximum height of this second peak belongs to the lowest concentration of methanol ($x_{\text{methanol}} = 0.1$). An analogous behavior was reported by Hanke and Lynden-Bell²⁴ in their simulation studies of mixtures of [DMIM][Cl] with water. In our computational simulations of IL/water mixtures,¹¹ we also found this second peak when the halogen anions were present, but its maximum height was registered for the highest water concentration. The different heights of the first peaks shown in Figure 7 imply that the interaction between alcohol molecules and anions is stronger in the case of the halogen anion than for the polyatomic ones, reproducing the same behavior that we previously detected in mixtures with water.¹¹

Thus, from analysis of the RDFs we can conclude that the alcohols interact preferentially with the IL anion, in agreement with previous computational studies of methanol/[BMIM][PF₆] mixtures performed by Canongia-Lopes et al.²⁸ The above figures show that hydrogen bonding between the alcohol molecules and the anions, responsible for the first peaks in the corresponding RDF, is stronger than the hydrogen bonding between alcohol molecules when the anion that is present in the mixture is the halogen one. Moreover, these hydrogen-bond interactions between the chloride and the alcohol are more pronounced for the shorter alcohol chain. Although in mixtures of ILs with water we reported the formation of a continuous water network that breaks the ionic network, in the mixtures with alcohols of the present paper the hydrogen bonding between the alcohol molecules does not seem to be relevant enough until very high alcohol molar fractions, whereas the strong interaction between alcohols and chloride anions suggests once again that alcohol molecules are homogeneously distributed in the IL network. These conclusions are reinforced by the analysis of the coordination numbers and average number of hydrogen bonds per alcohol molecule shown in the following.

The above conclusions can be reinforced analyzing the coordination numbers of alcohol molecules in the mixtures. The most usual way for evaluating coordination numbers in the literature is by numerical integration of the RDF $4\pi r^2 g(r)$ up to the first minimum. In order to test our results, we computed

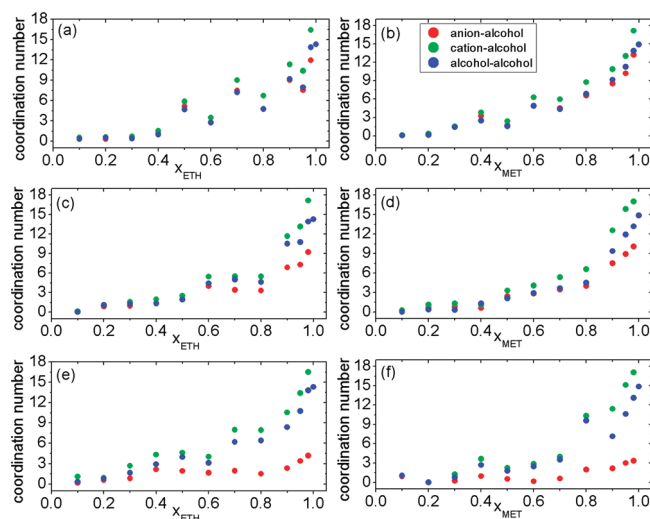


Figure 9. Coordination numbers of ethanol (a,c,e) and methanol (b,d,f) in mixtures with [HMIM][PF₆] (a,b), [HMIM][BF₄] (c,d), and [HMIM][Cl] (e,f) at 298.15 K.

the oxygen–hydrogen and oxygen–oxygen RDFs for liquid methanol and ethanol, and compared the obtained curves and the corresponding coordination numbers with those reported in previous computational simulations.⁵³ These curves are shown in Figure 8. The coordination numbers calculated by integration of the corresponding first peak were for pure methanol and ethanol 2.61 and 2.08, respectively, in the case of O–O pairs and 1.13 and 0.82 when using O–H pairs. Our calculated coordination numbers differ only slightly from the ones reported by Saiz et al.,⁵³ which are 2 and 1 for O–O and O–H pairs, respectively, but this property is known to be extremely sensitive to the choice of the position of the minimum. As one can see in this representation, sharp first peaks are registered for both alcohols both for O–H pairs and O–O pairs, followed by second broader peaks. Any appreciable correlation vanishes for $r > 0.6$ nm in both cases. Moreover, for O–O pairs, the first peaks are registered at 0.3 nm, 0.1 nm farther than for the former, reflecting the formation of hydrogen bonding in these systems (recall that a hydrogen bond is formed when the donor–acceptor distance is less than 0.35 nm, according to Gromacs criterion). It is also apparent in Figure 9 that our calculations predict slightly lower first peaks centered at larger distances of the central O atom for O–H pairs for both ethanol and methanol, and the same happens for the second peaks. This is also the case for O–O pairs, but in this case the maxima of our calculated second peaks are greater than those of Saiz et al. in ref 53, and the second neighbors are placed at slightly smaller distances.

In Figure 9 we represent the coordination numbers of alcohol/IL mixtures over the whole range of alcohol concentrations, obtained by integration of the first peak of the RDFs of the center of mass of the molecules, a less biased choice of distribution function. On the other hand, the number of methanol molecules surrounding another molecule of methanol is higher in mixtures with the PF₆⁻-based IL than in mixtures with [HMIM][Cl] up to high concentrations of alcohol ($x_{\text{methanol}} \approx 0.7$). This is in agreement with our previous statement that methanol molecules have a greater ability to coordinate with the halogen anion than with the more solvophobic one. Furthermore, Figure 9 shows that the number of ethanol molecules around another molecule

of ethanol in a mixture is higher than the methanol–methanol coordination number in the analogous mixture up to a high mole fraction of alcohol, which implies that methanol has a stronger interaction with anions than ethanol, as we concluded from our previous analysis of Figure 7. Moreover, we can compare our limiting Cl⁻–alcohol coordination numbers (4.2 and 3.4 for ethanol and methanol, respectively) with the value of 7.4 reported for water in our previous work for IL/water mixtures¹¹ (by way of comparison, 6 is the experimental value of aqueous chloride).⁵⁴ The limiting PF₆⁻–alcohol coordination number is 11.9 and 13.2 in mixtures with ethanol and methanol, respectively, while the value reported in our previous work in mixtures with water is 10.3.

The above discussion shows that calculation of coordination numbers by the usual method of integration under the first peak of an RDF involves a number of arbitrary choices. Furthermore, the information provided by the RDFs is limited by the fact that they lump together all the particles, so a certain degree of arbitrariness probably cannot be avoided unless a more detailed description is used. This issue has been discussed previously in the literature by McGreevy et al.⁵⁵ They calculated the coordination numbers of molten RbCl and LiI using a method based on a deconvolution of the RDFs obtained from simulations in terms of the partial RDFs $G(n,r)$ ($n = 1, 2, \dots$) defined as the probability density functions of finding the n th nearest neighbor of a particle at a distance r . Many parameters of these functions, such as peak position, height, width at half-height, and so forth can be used in order to determine whether a particular radial distribution curve is the last one of an inner coordination sphere, an intermediate one, or the first one of an outer sphere. However, McGreevy et al. showed that the best way to determine the boundary between two coordination spheres is as the distance where the ratio of the half-widths measured to either limit of the curves from their peak position is equal to unity. This technique has been used by subsequent authors to gain additional insight into the neighborhood relations present in systems with complex spatial correlations, such as in the study of liquid Bi by Souto et al.⁵² Accordingly, we also analyzed the partial RDFs of nearest neighbors up to a distance of around 0.63 nm, which is the distance of the first and second minimum of pure ethanol and methanol, respectively. From the computed $G(n,r)$, some of them plotted in Figure 10, we found that pure ethanol has 12 first neighbors, while pure methanol has two neighbors in the first shell and 13 neighbors in the second one, which is in agreement with the values previously plotted in Figure 9. Moreover, interestingly enough, these two shells of liquid methanol extend up to the same distance as the first shell of liquid ethanol. Some additional results for mixtures are shown in Table 2; it is noteworthy that [HMIM][Cl] in mixtures with methanol produces the disappearance of one of the two shells found in pure methanol, which is in agreement with the fact that RDFs of methanol/[HMIM][Cl] plotted in Figure 5 only show the first peak when high amounts of methanol are reached. It is also interesting to see the resonance of the first neighbor between the first two shells in mixtures of methanol/[HMIM][BF₄].

The criterion for defining a “hydrogen bond” in the context of computational simulations can be geometrical or energetic.⁵⁶ However, in the case of methanol, the choice is not as crucial as in other liquids such as water, and both criteria lead to almost identical results. According to ref 56, a pair of molecules are considered H-bonded if the distance between the hydrogen and the acceptor is smaller than 0.35 nm and the angle of the donor–hydrogen–acceptor is less than 30°. (According to the criterion

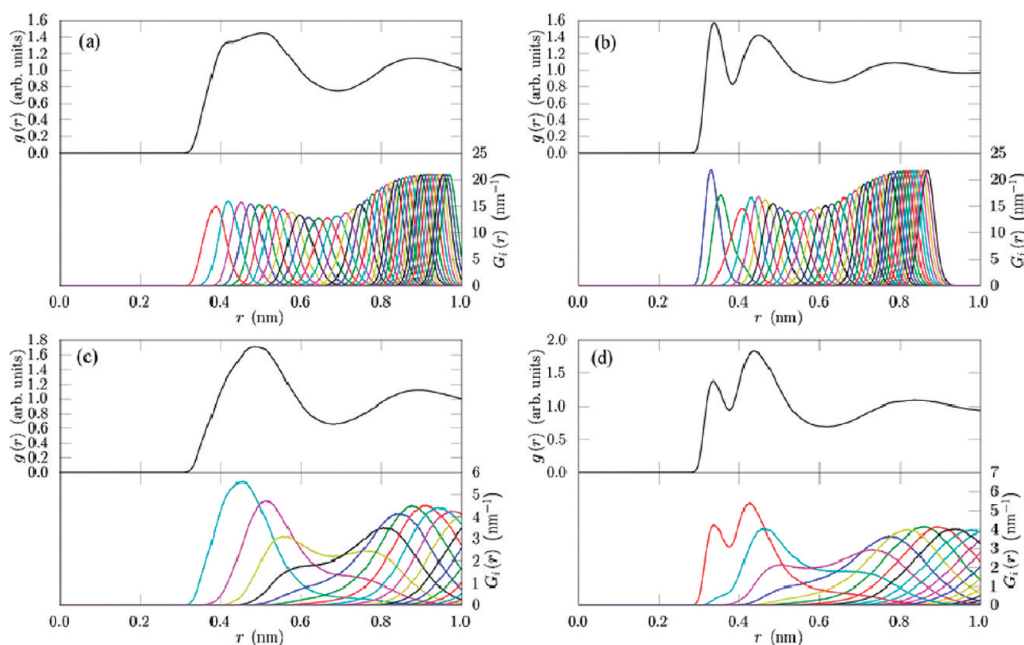


Figure 10. Deconvolution of the RDFs $g(r)$ in terms of the partial RDFs $G(n,r)$ ($n = 1, 2, \dots, 40$), corresponding to the first, second, third, etc., nearest neighbors in pure ethanol (a) and pure methanol (b), and in mixtures of ethanol (c) and methanol (d) with [HMIM][BF₄] at an alcohol content of $x_{\text{alcohol}} = 0.50$.

Table 2. Alcohol–Alcohol Coordination Numbers in Mixtures with [HMIM][PF₆], [HMIM][BF₄], and [HMIM][Cl] Derived from $G(n,r)$

	ethanol			methanol					
	$x_{\text{eth}} = 0.1$	$x_{\text{eth}} = 0.5$	$x_{\text{eth}} = 1.0$	$x_{\text{met}} = 0.1$		$x_{\text{met}} = 0.5$		$x_{\text{met}} = 1.0$	
	1 st shell	1 st shell	first shell	1 st shell	2 nd shell	1 st shell	2 nd shell	1 st shell	2 nd shell
HMIMPF ₆	1	3.5	12	1	1	2	3	2	13
HMIMBF ₄	1	3.5	12	1	1	1	3	2	13
HMIMCl	1	3.5	12	1	-	2.5	-	2	13

implemented in Gromacs, OH and NH groups are regarded as donors, and O and N are considered to be acceptors.) Figure 11 represents the cation–alcohol hydrogen bonding degree for all the analyzed mixtures together with their uncertainties calculated as the standard deviations of the mean of the stochastic series of hydrogen bonds in the time series of configurations. It can be seen there that the average number of hydrogen bonds per alcohol molecule is approximately 1 order of magnitude greater in mixtures with [HMIM][PF₆] and with [HMIM][BF₄] than with the halogen anion, probably due to the greater interaction between alcohol molecules and the chloride anion. On the other hand, maxima in the number of hydrogen bonds are observed in the case of mixtures of [HMIM][Cl] with both alcohols (Figure 11c). Although at very high concentration of alcohol ($x_{\text{solvent}} > 0.9$) the behavior of this magnitude is similar for all the studied compounds, below this concentration this number exhibits a relatively fast decrease in the case of the chlorinated IL, reflecting that most of the alcohol molecules in the bulk are bound to the other species in the mixture (anions or other alcohol molecules). Taking into account the results above, we can conclude that they are preferentially bound to chloride anions, what reflects once more that the affinity of Cl[−] to hydrogen bond

to both methanol and ethanol molecules is much greater than those of more hydrophobic anions such as PF₆[−] or BF₄[−].

Figure 12 shows the variable

$$\xi = \frac{n_{\text{alc-alc}}^{\text{mixture}}}{n_{\text{alc-alc}}^{\text{pure}}} \quad (4)$$

that is, the average number of alcohol–alcohol hydrogen bonds per alcohol molecule normalized to its value in pure alcohol for all the studied IL/alcohol mixtures in order to analyze the effect of the anion on the number of alcohol–alcohol hydrogen bonds. The average number of alcohol–alcohol hydrogen bonds in the pure system that appears as the denominator of eq 4 was computed to be 1.82 for both ethanol and methanol, in good agreement with the experimental value of approximately two hydrogen bonds per ethanol and methanol molecule.⁵⁷ This suggests the existence of linear chains of hydrogen bonded molecules of alcohol, a structure also reported in computational studies of liquid alcohols.^{35,53,56,58} As can be seen in Figure 12, the number of hydrogen bonds per alcohol molecule monotonically increases with the amount of alcohol. In the case of mixtures with water we reported in ref 11 a value of approximately 3.5 hydrogen bonds

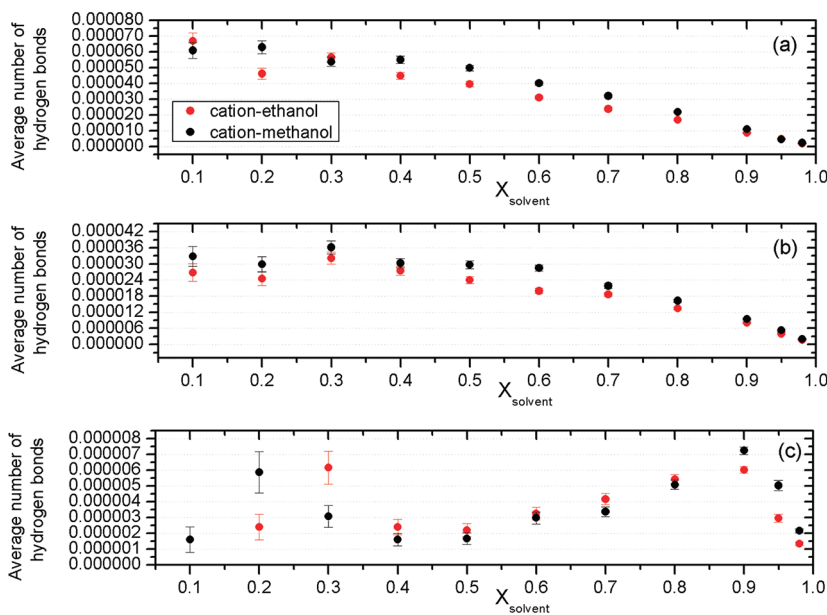


Figure 11. Concentration dependence of the average number of cation–alcohol hydrogen bonds per alcohol molecule for mixtures with [HMIM][PF₆] (a), [HMIM][BF₄] (b), and [HMIM][Cl] (c) at 298.15 K.

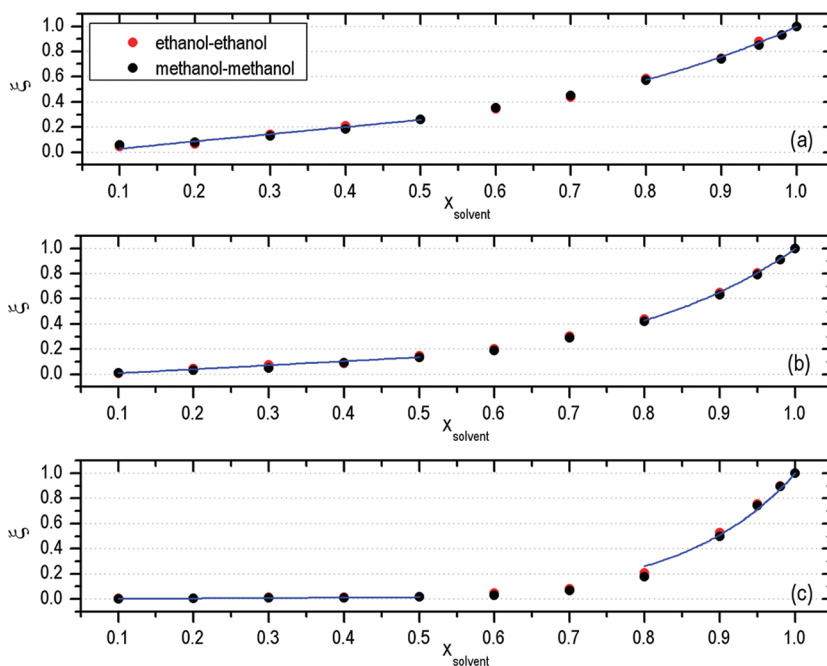


Figure 12. Concentration dependence of the average number of alcohol–alcohol hydrogen bonds per alcohol molecule normalized to its value in pure alcohol for mixtures with [HMIM][PF₆] (a), [HMIM][BF₄] (b), and [HMIM][Cl] (c) at 298.15 K. Also shown are linear (exponential) fits in the low (high) concentration range; see the text for details.

per water molecule in pure water, which is similar to the four hydrogen bonds of most water molecules in the liquid phase.^{59–61} On the other hand, the increase of the average number of alcohol–alcohol hydrogen bonds per alcohol molecule is notably slower for the chlorinated IL than for the other compounds throughout the whole range of concentrations. In fact, in [HMIM][Cl]/alcohol mixtures, ξ does not reach a value of 0.2 up to a content of alcohol around $x_{\text{alcohol}} \approx 0.8$, whereas that value is reached in [HMIM][BF₄]/alcohol mixtures at $x_{\text{alcohol}} \approx 0.6$, and in the

most solvophobic compound at $x_{\text{alcohol}} \approx 0.4$. This fact reinforces the notion of the existence of strong hydrogen bonding between alcohol molecules and the chloride anion. Hydrogen bonding between alcohol molecules is not relevant until high alcohol mole fractions in mixtures with hydrophilic anions, while in mixtures where the solvophobic anions are present the interaction between alcohol molecules themselves seems to be stronger than that between alcohol molecules and the polyatomic anions. The results in Figure 12c can be compared to those we previously

reported for mixtures with water (Figure 8b of ref 11). This comparison shows that the increase of average hydrogen bonding between solvent molecules is notably greater in mixtures of [HMIM][Cl] with water than in its mixtures with any of the alcohols. In mixtures with water the normalized average number of water–water hydrogen bonds is greater than 0.1 at $x_{\text{water}} \approx 0.5$, and greater than 0.4 at a mole fraction of water of approximately $x_{\text{water}} \approx 0.75$, whereas in mixtures of [HMIM][Cl] with alcohols these values of the alcohol–alcohol hydrogen bonding degree are not reached up to $x_{\text{alcohol}} \approx 0.75$ and $x_{\text{alcohol}} \approx 0.9$, respectively. This reflects once again that no alcohol network similar to the water network formed with increasing water concentration in IL/water mixtures occurs in mixtures of alcohol with [HMIM][Cl], where the alcohol molecules seem to be homogeneously placed in the polar network of IL. However, in mixtures where polyatomic anions are present, alcohol molecules tend to form bigger clusters that increase in size with increasing mole fraction of alcohol, until they percolate to form a network of large alcohol clusters at high amounts of alcohol.

The behavior of $\xi(x_{\text{solvent}})$ at both extremes of the concentration range can be explained in a semiquantitative fashion using simple models. At very low solvent concentrations, solvent molecules can be thought of as acting like in an ideal gas with $g(r) \approx 1$. Thus, the frequency of two of these molecules being close enough to form an hydrogen bond in this limit is roughly proportional to the density of the system (which in turn can be approximated by the density of the pure IL) and therefore linear in the mole fraction of solvent. This linear behavior is clearly observed in Figure 12, and in fact extends reasonably well up to intermediate concentrations. As expected, the slope of the corresponding linear fit is higher for denser ILs, and proportional to the density of the pure IL. At the other end of the concentration spectrum, the action of adding an ionic pair to pure solvent is followed by a solvation process involving a number of solvent molecules that are thus prevented from forming hydrogen bonds. The reduction in the total number of solvent–solvent hydrogen bonds is therefore proportional to the number of IL molecules introduced and to ξ . Using very simple approximations, this can be shown to yield a result of the form $\xi = e^{\gamma(x_{\text{solvent}} - 1)}$ valid for $x_{\text{solvent}} \approx 1$, with a parameter γ , which should be larger in those systems in which solvent–IL interactions are stronger. The corresponding exponential fits are also shown in Figure 12, and the values of γ (2.8 for [HMIM][PF₆], 4.2 for [HMIM][BF₄], and 6.7 for [HMIM][Cl]) follow the expected trend. The mismatch between the slopes of the linear and exponential regions is barely noticeable for [HMIM][PF₆], somewhat more marked for [HMIM][BF₄], and fairly accused for [HMIM][Cl], where two clearly different regimes can be observed. Interesting conclusions for the degree of clusterization can be drawn from this contrast: the fact that the linear regime is valid in such a wide range for [HMIM][Cl]/alcohol mixtures indicates that solvent molecules can be considered disaggregated up to very high concentrations, whereas the much earlier onset of bulk-like behavior in alcohol mixed with [HMIM][PF₆] points to the existence of large alcohol clusters (probably forming a network, which breaks the polar IL network) already at intermediate concentrations.

4. CONCLUSIONS

We performed MD simulations for binary mixtures of the imidazolium-based ILs [HMIM][PF₆], [HMIM][BF₄], and [HMIM][Cl] with methanol and ethanol, and we analyzed

several thermodynamic and structural properties of the system. Moreover, we studied the influence of the anion hydrophobicity degree, the length of the molecular chain of the alcohol, and of the concentration of alcohol on the evolution of the microstructure of the mixtures. In particular, we have analyzed densities, excess molar volumes, total and partial RDFs, coordination numbers, and average degrees of hydrogen bonding of the species present in the mixtures.

To check the reliability of the force field employed, we calculated the densities of pure ILs and alcohols and compared them to experimental values. Our simulated densities show a maximum deviation from the experimental ones of 1.79%. Additionally, the densities of the mixtures were in good agreement with the experimental data available in the literature. In order to quantify the nonideality of the mixtures, we determined the excess molar volumes of mixing, which were negative for all the mixtures over the whole range of concentrations due to the intermolecular forces between the components of the mixture and the packing effect due to the different shapes and sizes of the molecules. We observed that alcohol molecules are more densely packed in mixtures with Cl⁻ than in mixtures with PF₆⁻ and BF₄⁻, and that methanol molecules show a better packing than ethanol ones.

The RDFs of the mixtures showed that the interaction between anions and alcohols increases in the order Cl⁻ > BF₄⁻ > PF₆⁻. Moreover, this interaction is more significant for methanol than for ethanol. Additionally, there is no aggregation of alcohol molecules around the cationic part of ILs. Significant hydrogen bonding between alcohol molecules does not come up until high concentrations of alcohols in the presence of the chloride anion. Thus, whereas in mixtures with water we reported the formation of a water network that breaks the polar network, in mixtures with alcohols the alcohol molecules are homogeneously distributed in the structure of the chloride-based IL. However, in the more solvophobic mixtures with fluorinated anions our results seem to be compatible with the formation of some kind of network. This aggregation trend was confirmed by the analysis of the evolution of the coordination number and the average number of hydrogen bonds per alcohol molecule with the mole fraction of alcohols. Moreover, the study of these two properties show that [HMIM][PF₆]/alcohol mixtures form clusters of alcohol molecules whose size increases with increasing mole fraction of alcohol and it is bigger than in [HMIM][Cl]/alcohol mixtures but smaller than in mixtures of [HMIM][PF₆] with water.

A systematic study of the dynamic properties of these mixtures, including their diffusion coefficients and the velocity autocorrelation functions, is now in progress.

■ AUTHOR INFORMATION

Corresponding Author

*E-mail address: luismiguel.varela@usc.es.

■ ACKNOWLEDGMENT

The authors wish to acknowledge the financial support of the Xunta de Galicia through the research projects of references 10 PXIB 103 294 PR and 10 PXIB 206 294 PR. Moreover, this work has been funded by the Spanish Ministry of Science and Innovation (Grant No. FIS2008-04894/FIS). All these research projects are partially supported by FEDER. J.C. and T.M.-M. thank the Spanish ministry of Education for their FPU grants.

Facilities provided by the Galician Supercomputing Centre (CESGA) are also acknowledged.

■ REFERENCES

- (1) Wilkes, J. S. *Green Chem.* **2002**, *4*, 73–80.
- (2) Earle, M. J.; Esperança, J. M. S. S.; Gilea, M. A.; Canongia-Lopes, J. N.; Rebello, L. P. N.; Magee, J. W.; Seddon, K. R.; Widgren, J. A. *Nature (London, U.K.)* **2006**, *439*, 831–834.
- (3) Chenfeng, Y.; Weimin, L.; Yunxia, C.; Laogui, Y. *Chem. Commun.* **2001**, *21*, 2244–2245.
- (4) Wakai, C.; Oleinikova, A.; Ott, M.; Weingärtner, H. *J. Phys. Chem. B* **2005**, *109*, 17028–17030.
- (5) Rogers, R. D.; Seddon, K. R. *Science* **2003**, *302*, 792–793.
- (6) Rogers, R. D.; Seddon, K. R. *Ionic Liquids as Green Solvents: Progress and Prospects*; ACS Symposium Series, 856; American Chemical Society: Washington, DC, 2003.
- (7) Rogers, R. D.; Seddon, K. R. *Ionic Liquids, Industrial Applications to Green Chemistry*; ACS Symposium Series, 818; American Chemical Society: Washington, DC, 2002.
- (8) Welton, T. *Chem. Rev. (Washington DC, U.S.)* **1999**, *99*, 2071–2084.
- (9) Carmichael, A. J.; Seddon, K. R. *J. Phys. Org. Chem.* **2000**, *13*, 591–595.
- (10) Hagiwara, R.; Ito, Y. *J. Fluorine Chem.* **2000**, *105*, 221–227.
- (11) Méndez-Morales, T.; Carrete, J.; Cabeza, O.; Gallego, L. J.; Varela, L. M. *J. Phys. Chem. B* **2011**, *115*, 6995–7008.
- (12) Cabeza, O.; Segade, L.; García-Garabal, S.; Rilo, E.; Domínguez-Pérez, M.; Varela, L. M. In *Ionic Liquids, Theory and Applications*; Intech: Rijeka, Croatia, 2011; pp 111–136.
- (13) Pereiro, A. B.; Rodríguez, A. *J. Chem. Eng. Data* **2007**, *52*, 1408–1412.
- (14) Sahandzhieva, K.; Tuma, D.; Breyer, S.; Kamps, A. P. S.; Maurer, G. *J. Chem. Eng. Data* **2006**, *51*, 1516–1525.
- (15) Crosthwaite, J. M.; Aki, S. N. V. K.; Maggin, E. J.; Brennecke, J. F. *J. Phys. Chem. B* **2004**, *108*, 5113–5119.
- (16) Pereiro, A. B.; Rodríguez, A. *J. Chem. Thermodyn.* **2007**, *39*, 978–989.
- (17) Domanska, U.; Marciniak, A. *J. Phys. Chem. B* **2004**, *108*, 2376–2382.
- (18) Huo, Y.; Xia, S.; Ma, P. *J. Chem. Eng. Data* **2007**, *52*, 2077–2082.
- (19) Gómez, E.; González, B.; Calvar, N.; Tojo, E.; Domínguez, A. *J. Chem. Eng. Data* **2006**, *51*, 2096–2102.
- (20) Pereiro, A. B.; Tojo, E.; Rodríguez, A.; Canosa, J.; Tojo, J. *J. Chem. Thermodyn.* **2006**, *38*, 651–661.
- (21) Stoppa, A.; Hunger, J.; Buchner, R. *J. Chem. Eng. Data* **2009**, *54*, 472–479.
- (22) Gómez, E.; Calvar, N.; Domínguez, I.; Domínguez, A. *Phys. Chem. Liq.* **2006**, *44*, 409–417.
- (23) Rilo, E.; Pico, J.; García-Garabal, S.; Varela, L. M.; Cabeza, O. *Fluid Phase Equilib.* **2009**, *285*, 83–89.
- (24) Hanke, C. G.; Lynden-Bell, R. M. *J. Phys. Chem. B* **2003**, *107*, 10873–10878.
- (25) Jiang, W.; Wang, Y.; Voth, G. A. *J. Phys. Chem. B* **2007**, *111*, 4812–4818.
- (26) Feng, S.; Voth, G. A. *Fluid Phase Equilib.* **2010**, *294*, 148–156.
- (27) Hanke, C. G.; Atamas, N. A.; Lynden-Bell, R. M. *Green Chem.* **2002**, *4*, 107–111.
- (28) Canongia-Lopes, J. N.; Costa-Gómez, M. F.; Pádua, A. A. H. *J. Phys. Chem. B* **2006**, *110*, 16816–16818.
- (29) Raabe, G.; Köhler, J. *J. Chem. Phys.* **2008**, *129*, 144503(1)–144503(8).
- (30) Jahangiri, S.; Taghikhani, M.; Behnejad, H.; Ahmadi, S. *J. Mol. Phys.* **2008**, *8*, 1015–1023.
- (31) Heintz, A.; Ludwig, R.; Schmidt, E. *Phys. Chem. Chem. Phys.* **2011**, *13*, 3268–3273.
- (32) Huddleston, J. G.; Visser, A. E.; Reichert, W. M.; Willauer, H. D.; Broker, G. A.; Rogers, R. D. *Green Chem.* **2001**, *3*, 156–164.
- (33) Holbrey, J. D.; Seddon, K. R. *J. Chem. Soc., Dalton Trans.* **1999**, 2133–2139.
- (34) Spoel, D. V. D.; Lindahl, E.; Hess, B.; Buuren, A. R. V.; Apol, E.; Meulenhoff, P. J.; Tielemans, D. P.; Sijbers, A. L. T. M.; Feenstra, K. A.; Drunen, R. V.; Berendsen, H. J. C. *Gromacs User Manual, version 4.0*. <http://www.Gromacs.org>, 2005.
- (35) Jorgensen, W. L. *J. Phys. Chem.* **1986**, *90*, 1276–1284.
- (36) Sambasivaram, S. V.; Acevedo, O. *J. Chem. Theory Comput.* **2009**, *5*, 1038–1050.
- (37) Prado, C. E. R.; Freitas, L. C. G. *J. Mol. Struct.* **2007**, *847*, 93–100.
- (38) Canongia-Lopes, J. N.; Deschamps, J.; Pádua, A. A. H. *J. Phys. Chem. B* **2004**, *108*, 2038–2047.
- (39) Bayly, C. I.; Cieplak, P.; Cornell, W.; Kollman, P. A. *J. Phys. Chem.* **1993**, *97*, 10269–10280.
- (40) Brenneman, C. M.; Wilberg, K. B. *J. Comput. Chem.* **1990**, *11*, 361–373.
- (41) Frisch, M. J.; Trucks, G. W.; Schlegel, H. B.; Gill, P. M. W.; Johnson, B. G.; Robb, M. A.; Cheeseman, J. R.; Keith, T.; Petersson, T. G. A.; Montgomery, J. A.; Raghavachari, K.; Al-Laham, M. A.; Zakrzewski, V. G.; Ortiz, J. V.; Foresman, J. B.; Peng, C. Y.; Ayala, P. A.; Wong, M. W.; Andres, J. L.; Replogle, E. S.; Gomperts, R.; Martin, R. L.; Fox, D. J.; Binkley, J. S.; Defrees, D.; Baker, J.; Stewart, J. P.; Head-Gordon, M.; Gonzalez, C.; Pople, J. A. *Gaussian 94*, revision A.1; Gaussian, Inc.: Pittsburgh, PA, 1995.
- (42) Jorgensen, W. L.; Maxwell, D. S.; Tirado-Rives, J. *J. Am. Chem. Soc.* **1996**, *118*, 11225–11236.
- (43) Darden, T.; York, D.; Pedersen, L. *J. Chem. Phys.* **1993**, *98*, 10089–10094.
- (44) Hess, B.; Bekker, H.; Berendsen, H. J. C.; Fraaije, J. G. E. M. *J. Comput. Chem.* **1997**, *18*, 1463–1472.
- (45) Hess, B. *J. Chem. Theory Comput.* **2007**, *4*, 116–122.
- (46) Micaelo, N. M.; Baptista, A. M.; Soares, C. M. *J. Phys. Chem. B* **2006**, *110*, 14444–14451.
- (47) Bussi, G.; Donadio, D.; Parrinello, M. *J. Chem. Phys.* **2007**, *126*, 014101(1)–014101(7).
- (48) Parrinello, M.; Rahman, A. *J. Appl. Phys.* **1981**, *52*, 7182–7190.
- (49) Gómez, E.; González, B.; Domínguez, A.; Tojo, E.; Tojo, J. *J. Chem. Eng. Data* **2006**, *51*, 696–701.
- (50) Gibson, H. M.; Wilding, N. B. *Phys. Rev. E* **2006**, *73*, 061507.
- (51) Kelkar, M. S.; Shi, W.; Maginn, E. J. *Ind. Eng. Chem. Res.* **2008**, *47*, 9115–9126.
- (52) Souto, J.; Alemany, M. M. G.; Gallego, L. J.; González, L. E.; González, D. *Phys. Rev. B* **2010**, *81*, 134201.
- (53) Saiz, L.; Padró, J. A.; Guàrdia, E. *J. Phys. Chem. B* **1997**, *101*, 78–86.
- (54) Stuart, S. J.; Berne, B. J. *J. Phys. Chem.* **1996**, *100*, 11934–11943.
- (55) McGreevy, R. L.; Baranyai, A.; Ruff, I. *Phys. Chem. Liq.* **1986**, *16*, 47–54.
- (56) Haughney, M.; Ferrario, M.; McDonald, I. R. *J. Phys. Chem.* **1987**, *91*, 4934–4940.
- (57) Yamaguchi, T.; Hidaka, H.; Soper, A. K. *Mol. Phys.* **1999**, *96*, 1159–1168.
- (58) Matsumoto, M.; Gubbins, K. E. *J. Chem. Phys.* **1990**, *93*, 1981–1994.
- (59) Guo, J. H.; Luo, Y.; Augustsson, A.; Rubensson, J. E.; Sathe, C.; Agren, H.; Siegbahn, H.; Nordgren, J. *Phys. Rev. Lett.* **2002**, *89*, 137402.
- (60) Luzar, A.; Chandler, D. *Phys. Rev. Lett.* **1996**, *76*, 928–931.
- (61) Stillinger, F. H. *Science* **1980**, *209*, 451–457.